

Measuring competitive exclusion in non-small cell lung cancer

Nathan Farrokhanian^{1,+}, Jeff Maltas^{2,+}, Mina Dinh², Arda Durmaz¹, Patrick Ellsworth¹, Masahiro Hitomi², Erin McClure², Andriy Marusyk³, Artem Kaznatcheev^{4,*}, and Jacob G Scott^{1,2,5,*}

¹Case Western Reserve School of Medicine, Cleveland, OH, USA

²Department of Translational Hematology and Oncology Research, Cleveland Clinic, Cleveland, OH, USA

³Department of Cancer Physiology, Moffitt Cancer Center, Tampa, FL, USA

⁴Department of Biology, University of Pennsylvania, Philadelphia, PA, USA

⁵Department of Radiation Oncology, Cleveland Clinic, Cleveland, OH, USA

*corresponding authors: scottj10@ccf.org, kaznatcheev.artem@gmail.com

+these authors contributed equally to this work

ABSTRACT

Therapeutic strategies for tumor control have traditionally assumed that maximizing reduction in tumor volume correlates with clinical efficacy. Unfortunately, this rapid decrease in tumor burden is almost invariably followed by the emergence of therapeutic resistance. Evolutionary based treatment strategies attempt to delay resistance via judicious treatments that maintain a significant treatable subpopulation. While these strategies have shown promise in recent clinical trials, they often rely on biological conjecture and intuition to derive parameters. In this study we experimentally measure the frequency-dependent interactions between a gefitinib resistant non-small cell lung cancer (NSCLC) population and its sensitive ancestor via the evolutionary game assay. We show that cost of resistance is insufficient to accurately predict competitive exclusion and that frequency-dependent growth rate measurements are required. In addition, we show that frequency-dependent growth rate changes may ultimately result in a safe harbor for resistant populations to safely accumulate, even those with significant cost of resistance. Using frequency-dependent growth rate data we then show that gefitinib treatment results in competitive exclusion of the ancestor, while absence of treatment results in a likely, but not guaranteed exclusion of the resistant strain. Finally, using our empirically derived growth rates to constrain simulations, we demonstrate that incorporating ecological growth effects can dramatically change the predicted time to sensitive strain extinction. In addition, we show that higher drug concentrations may not lead to the optimal reduction in tumor burden. Taken together, these results highlight the potential importance of frequency-dependent growth rate data for understanding competing populations, both in the laboratory and the clinic.

¹ Introduction

² Given our current understanding of intratumoral heterogeneity, treatment resistance after continuous drug dose is an expected consequence. Genomic instability¹, inherent to the development of most cancer^{2–5}, results in the accumulation of a variety of aberrations within a single tumor population.⁶ While only a small subset of these randomly distributed changes will contribute directly to driving carcinogenesis, this diverse population comprised of phenotypically distinct subclones results in increased resilience of the overall tumor population across a wide range of external stressors.^{7,8}

⁷ These distinct subclones do not live, grow, or reproduce in isolation, however. With this diverse cellular population comes a diverse range of intercellular interactions including competition⁹ and cooperation between cancer cells¹⁰ and complex interactions with the microenvironment^{11–13}. Complex systems cannot often be fully described empirically, and their dynamics can be difficult to intuit from measurements of their parts. In these situations, mathematical models have historically played a role. Specifically, evolutionary game theory has been effective in predicting the evolutionary consequences of interactions in

12 large multicellular ecosystems, such as fisheries¹⁴ and game reserves.¹⁵ More recently, these evolutionary game theoretical
13 models have been used to gain insight into phenotypic shifts that occur within tumor ecosystems.^{12,16–18} As a consequence, we
14 must understand both the absolute fitness advantages of particular subpopulations in the selecting environment (monoculture),
15 as well as how competing clones modulate that advantage as a function of population frequency (co-culture).¹⁹ This frequency-
16 dependent growth can drastically expand what challenges evolution can adapt to²⁰ and acts to shape treatment-naïve tumor
17 ecosystems and influences inevitable development of resistance in post-treatment environments.^{9,21–23} As traditional treatment
18 protocols continue to fail, more evolutionary-based treatments that rely on judicious treatment schedules and cooperative
19 dynamics between populations have gained in popularity.^{11,24–33}

20 Dynamic therapeutic protocols using models of this type have already made their way into the clinic with promising
21 results.²⁷ While this highlights the value of game theoretical models for treatment optimization, the specific model in this, and
22 other clinical trials have been selected and parameterized mainly based on biological conjecture and intuition.^{34,35} Instead, for
23 each clinical condition, a different model and parameters would likely be needed to accurately capture intratumoral dynamics.
24 As such, reproducibility of this initial success across different tissues and environmental contexts is contingent on our ability to
25 measure subclonal interactions in the lab prior to transitioning to clinical practice. These interactions can greatly influence the
26 evolutionary trajectory of the tumor; therefore, incorrect characterization could unintentionally worsen treatment outcomes.

27 One such concept that is frequently assumed to be the driver of inevitable treatment resistance within these models is that of
28 competitive release.³⁶ This phenomenon was first described by Joseph Connell while studying the distribution of barnacles
29 off the shore of Millport, Scotland, where it was observed that two species occupied two distinct horizontal zones on the
30 shoreline.³⁷ Connell determined that the upper species, *Chthamalus stellatus*, was competitively excluded from populating
31 the lower region as a result of competitive interactions with the lower species, *Balanus balanoides*. Experimental removal of
32 *Balanus* by Connell released *Chthamalus* from this competitive exclusion, which resulted in expansion into the lower horizontal
33 zone. Similarly, in tumors, it is thought that selective killing of sensitive cells during therapy removes competitive restrictions
34 on resistant populations, allowing for their outgrowth and subsequent therapeutic failure. While intuitive in theory and observed
35 in bacteria³⁸ and parasites^{39–41}, empirical evidence of the dynamics that underlie this phenomenon in cancer have, to our
36 knowledge, yet to be elucidated.

37 As a population becomes increasingly resistant to a new treatment, it is common for that population to pay a ‘fitness
38 cost’ to maintain that resistant mechanism, leading to a reduced growth rate when compared to the ancestor from which it
39 was derived.^{42,43} This has led many researchers to suggest that the sensitive ancestor is likely to out-compete the resistant
40 clone when selection is removed, and thus treatment holidays may be beneficial to the maintenance of a treatable cancer
41 population^{12,27}. In some cases the fitness cost may be significant enough to result in competitive exclusion of the resistant
42 strain upon treatment withdrawal. In this work we consider the importance of empirical, frequency-dependent growth rate
43 measurements in identifying competitive exclusion. Beginning with PC9, a model cancer system for EGFR TKI resistance
44 in NSCLC, we show that competitive exclusion requires one population to out-compete (have a higher growth rate than)

another population under all possible population frequencies. We then measure these frequency-dependent growth rates for a gefitinib-resistant population and the ancestor from which it was derived and show that competitive exclusion is likely, but not guaranteed. We then show that the addition of gefitinib shifts the frequency-dependent growth rates such that the resistant strain will competitively exclude the ancestor at all tested concentrations. Finally, combining our empirically derived growth measurements with traditional competition simulations, we demonstrate that the inclusion of ecological effects can significantly alter the predicted time to exclusion of the ancestor, and thus alter the time required to reach an untreatable resistant tumor. In addition, we show that contrary to the maximal tolerable dose hypothesis, higher drug doses may not constrain tumor burden better than lower doses for our system.

Results

Ecological interactions ameliorate some, but not the entire fitness cost associated with resistance, resulting in competitive exclusion of the resistant population in the absence of treatment.

We investigated the evolutionary games (frequency-dependent ecological interactions) between sensitive and gefitinib-resistant cell lines in the lung adenocarcinoma cell line PC9. To create the resistant line, we exposed the population to 1 μM gefitinib for 6 months. In parallel, the original sensitive PC9 cell line was propagated in a matched volume of DMSO for 6 months. To recapitulate the clinical scenario, upfront treatment with high escalated dose was chosen over dose escalation protocol. We then used the game assay we have previously developed to quantify ecological interactions between populations.³⁰. Briefly, we co-cultured the derived gefitinib resistant cell line, with the DMSO propagated sensitive cell line at varying sensitive population to resistant population ratios (Fig 1A) in a 96 well plate. Using an automated incubator (BioTek Biospa) and time lapse microscopy setup, we imaged the wells every 4 hours. Cell lines were transduced with EGFP and mCherry fluorescent proteins that, when combined with image processing software, allowed for quantification of population level cell counts, and therefore population growth rates (Fig 1B). Then, by combining the parallel experiments done at varying initial sensitive populations, we can plot the frequency dependent growth rates for both the resistant and sensitive cell lines (Fig 1C). Finally, we can extract the payoff matrix that describes the evolutionary game dynamics as shown in Fig 1D.

In addition to the frequency-dependent growth rate measurements based on heterogeneous (mixed sensitive and resistant populations), we also performed the more standard measure, of the homogeneous, monotypic growth rates for both cell lines in DMSO. In this case, there is a substantial growth cost to the resistant phenotype, which grows at roughly three-fourths (75.6%) the rate of the monotypic sensitive PC9 population (Fig 2B, left panel). Fitness costs are often assumed in treatment resistant populations of EGFR driven NSCLC,⁴⁴ however this feature may not be generalizable across all NSCLC types.³⁰ While it is tempting to extrapolate this data and suggest these growth rate differences necessitate competitive exclusion of the resistant cell line due to its lower growth in DMSO, this is not necessarily so. Ecological interactions between the populations can ameliorate the fitness cost associated with resistance as shown in the left panel of cartoon plot, Fig 2A. The difference between the resistant and ancestor population's frequency-dependent growth rate is known as the gain function. For competitive exclusion to occur,

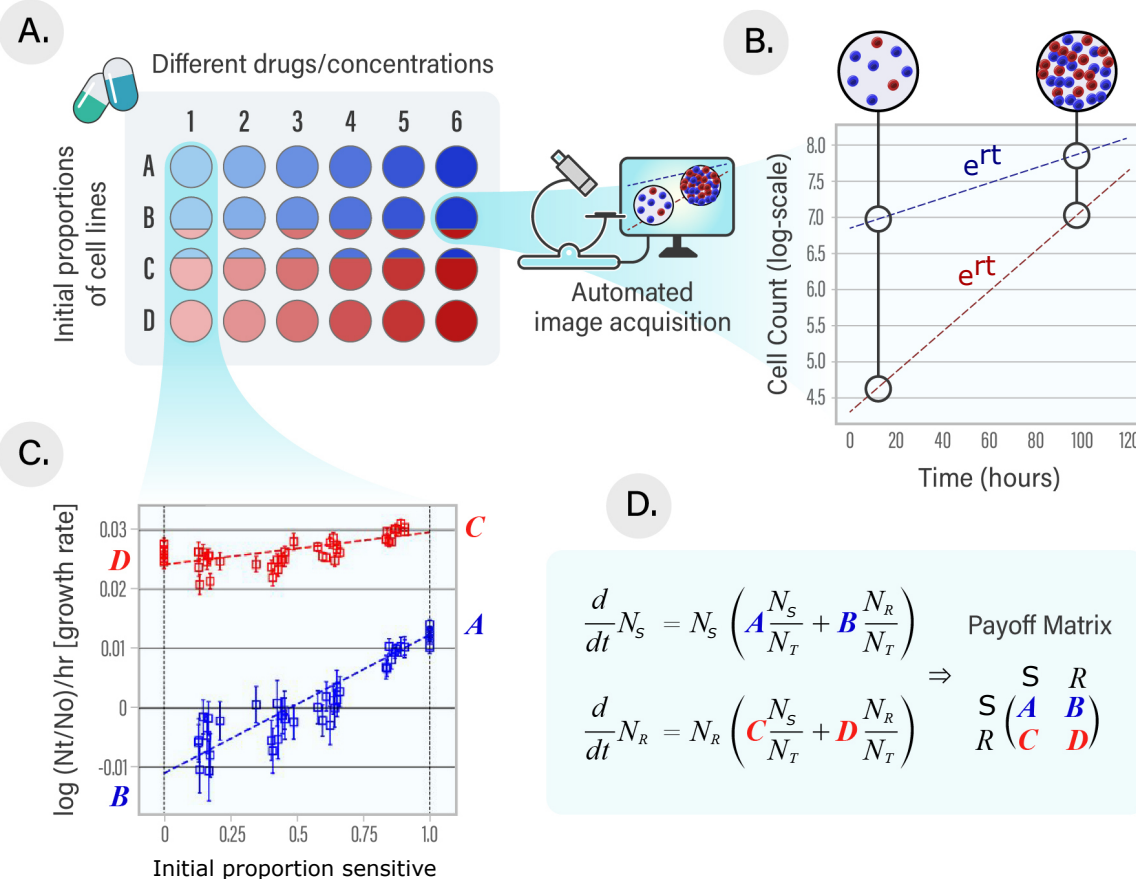


Figure 1. Experimental design for evolutionary game assay. (A) To track differential growth dynamics of two populations in the same culture, each population was transduced with a vector encoding a different heritable fluorescent protein. A Gefitinib-resistant cell line (red) and its sensitive ancestor (blue) were plated across a full spectrum of initial proportions (A, B, C, D...) and in a range of different different drugs and concentrations (1, 2, 3, 4...) in a 96 well plate. (B) Automated time-lapse microscopy imaging captures the composition of the population in each well every four hours. Cell number counts were extracted from each fluorescent image and plotted against elapsed time to derive growth rates in each well for each population via semi-log regression using the Theil-Sen estimator. (C) Extracted growth rates were then plotted against the seeded proportion of sensitive cells in the population (i.e. $p = N_S/N_T$; where N_S is the sensitive population size and N_T is the total population size) for each well. To find the fitness functions, least squares regressions (weighted against the inverse of the errors associated with each growth rate) was performed on this data. The resulting linear equations are the fitness functions $\hat{w}_S = Ap + B(1-p)$ and $\hat{w}_R = Cp + D(1-p)$. (D) Payoff matrices corresponding to each of the different conditions were derived from the resulting fitness functions to clearly represent the fitness outcome of specific interactions using least squared regression and intercepts of $p = 0$ and $p = 1$. For example, the fitness outcome of sensitive cells interacting with one another occurs when $p = 1$, which translates to $\hat{w}_S = A$. Similarly, the fitness outcome of when sensitive interacts with resistant occurs when $p = 0$, which translates to $\hat{w}_S = B$. For more details on the game assay, see Ref.³⁰ for method and Ref.³⁴ for interpretation.

77 the value of the gain function cannot change sign for any population frequency. That is, if the gain function is positive (or
 78 negative), it must remain positive (or negative) for all population frequencies. If instead the gain function transitions from
 79 negative to positive, or vice versa, a fixed point will occur.⁴⁵ If the fixed point is stable (negative to positive gain) then it will
 80 allow for co-existence of both populations, while the opposite (positive to negative gain) leads to an unstable fixed point.

81 Our experiments reveal the ancestor out-competes the resistant population at all population frequencies, likely resulting
 82 in a complete competitive exclusion of the resistant population (**Fig 2B**, right panel). To confirm these were not a result of

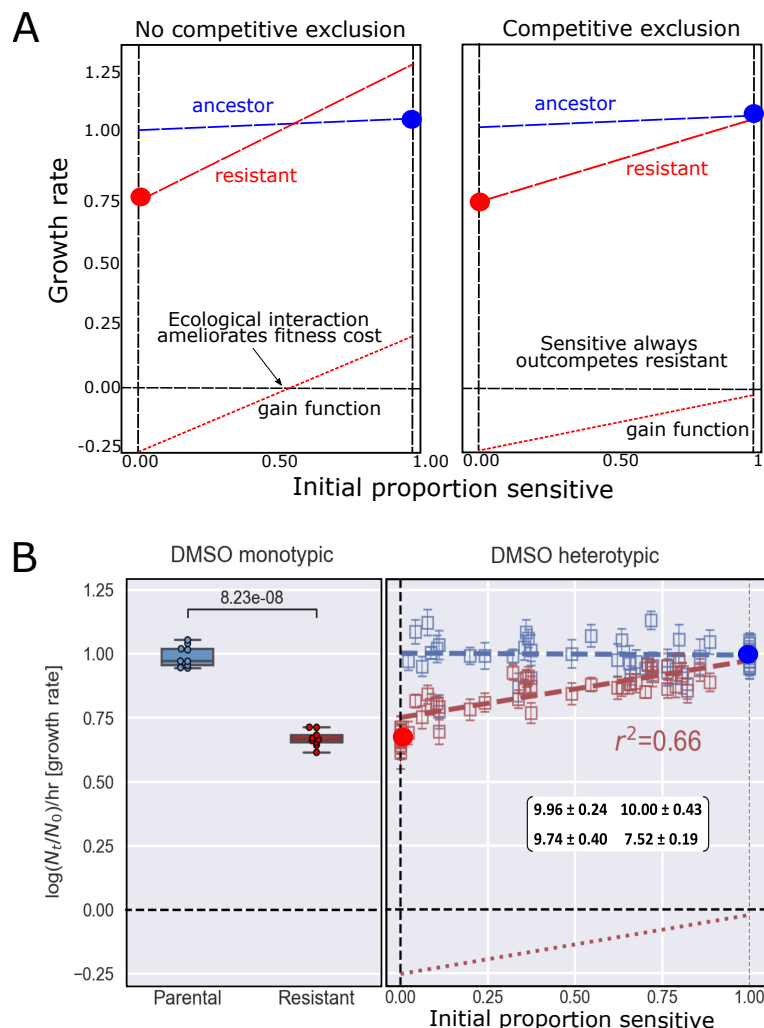


Figure 2. Ecological interactions alter but do not ameliorate the resistant clones fitness cost and result in competitive exclusion of the resistant strain in DMSO. **A.** Monotypic growth measurements are insufficient to predict competitive exclusion. The left and right panel both depict a resistant strain with a significant fitness cost associated with its resistance. Red circle at $p = 0$ represents monotypic resistant growth, while the blue circle at $p = 1$ represents monotypic sensitive growth. **Left Panel:** We see the ecological interaction is large enough to overcome the fitness cost when co-cultured with a majority sensitive population, resulting in no competitive exclusion. **Right Panel:** While there is significant ecological interaction, it is insufficient to overcome the fitness cost, resulting in complete competitive exclusion. **B. Left panel:** Monocultures in DMSO shows significant difference in growth between subclones ($p << 0.001$), highlighting the cost associated with the resistant phenotype. **Right panel:** Heterotypic cultures in DMSO reveal strong frequency-dependent interactions that modulate the resistant populations growth, however these ecological forces are insufficient to completely overcome the monoculture fitness cost, leading to competitive exclusion of the resistant subclone. The ancestor's growth remains consistent at all frequencies. Plotted values were normalized against mean monotypic sensitive growth in DMSO. Values in displayed game matrix have been scaled by a factor 10 for ease of comparison.

83 density-dependent growth effects (analogous to the inoculum effect in antibiotic resistance ⁴⁶), we measured the monoculture
 84 growth of both the sensitive and resistant population across a series of two-fold dilutions (**Figs S1, S4**). However, our co-culture
 85 experiments indicate the opposite — the **resistant population grows significantly faster at lower resistant population densities**,
 86 **suggesting the observed co-culture effects are not due to density-dependent monoculture interactions**. In addition, using the raw
 87 growth data, we show the co-culture data is not well fit by a model of exponential growth that ignores ecological dynamics
 88 (**Figs S2, S3**). In both populations, increasing density resulted in a slightly positive effect on growth.

89 Interestingly, however, the fitness cost of the resistant population is almost entirely ameliorated by ecological interactions
90 occurring at high sensitive population frequencies. Because this interaction occurs at resistant population fractions near zero
91 that are hard to reliably measure empirically, it is possible that the resistant population is not completely competitively excluded,
92 and a fixed point may exist at this extreme. If this were to be the case, it could highlight one potential way a sensitive population
93 may generate and maintain drug-resistant populations without losing population-level fitness, as the resistant strain with a
94 significantly fitness cost could be maintained at low population frequency in the absence of drug.

95 **The addition of drug switches which population is competitively excluded.**

96 Next we sought to quantify the ecological interaction between the sensitive and resistant cell lines under the application of
97 increasing gefitinib concentrations (**Fig 3A, S5**). Interestingly, we see that as the concentration of gefitinib increases, the slopes
98 of the frequency-dependent growth rates (and therefore, ecological interaction magnitude) also increases. We can quantify
99 this more clearly by instead plotting the gain function, or the difference between the growth of the ancestor and resistant
100 cell lines (**Fig 3B**). When visualized this way, it is immediately apparent that under treatment of DMSO the resistant strain
101 is competitively excluded by the sensitive strain (blue line is completely above x-axis). In addition, we can conclude under
102 the treatment of all tested gefitinib concentrations the cell line that is out-competed is reversed, and the sensitive strain is
103 competitively excluded (all other lines are completely below the x-axis). Finally, we can see the slope changes from negative
104 for DMSO to increasingly positive as the concentration of gefitinib increases. This depicts an increasing ecological interaction
105 strength.

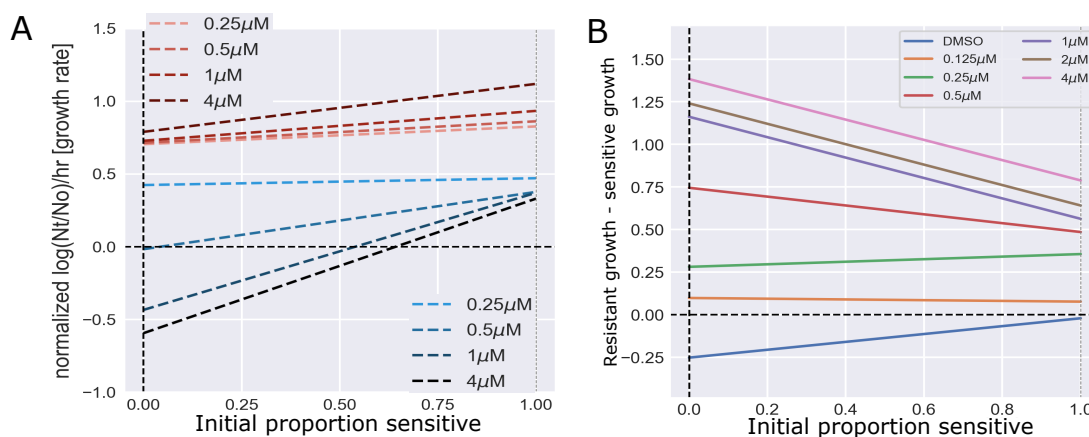


Figure 3. Increasing gefitinib concentration switches which population is competitively excluded from resistant to ancestor. A. Frequency-dependent growth rates were measured for several concentrations of gefitinib for both gefitinib-resistant (red) and the sensitive ancestor (blue). Growth values were normalized against the ancestor's mean monotypic growth in DMSO. Under all concentrations tested we see the resistant strain out-competing the ancestor at all population fractions, resulting in competitive exclusion of the ancestor. **B.** Gain function (growth of resistant cell line - growth of sensitive cell line) for all seven tested concentrations of gefitinib. DMSO's (blue) gain function exists entirely above $y = 0$ signifying competitive exclusion of the resistant cell line. For all non-zero concentrations the game dynamics shift to exist entirely below $y = 0$, indicating competitive exclusion of the sensitive strain.

106 **Competition simulations reveal importance of ecological effects in sensitive extinction rates and tumor
107 burden calculations.**

108 We built two kinds of mathematical models to explore the outcomes of sensitive extinction rates and tumour burden further. We
109 extrapolated the derived fitness functions out through time using both replicator dynamics (eq. 6) and a practical derivative of
110 the Lotka-Volterra (LV) equation (eq. 8) that allows for competitive exclusion of interacting species and better modelling of the
111 timescales of extinction dynamics⁴⁷. Both of these models attempt to predict population trends through time. The replicator
112 dynamics does this while modelling only frequency change and not population size³⁴. The LV model constrains the population
113 to a strict user-chosen carrying capacity or maximum size. *In vivo* tumor growth likely falls somewhere in between, as nutrient
114 availability and space constrains growth in a more fluid manner through mechanisms such as angiogenesis. For each model,
115 relative time to extinction was determined for the range of doses, where extinction is defined as proportion of the population, p ,
116 falling below < 0.01 . As expected, both models predict faster extinction of the sensitive population at higher doses (Fig 4A,B).

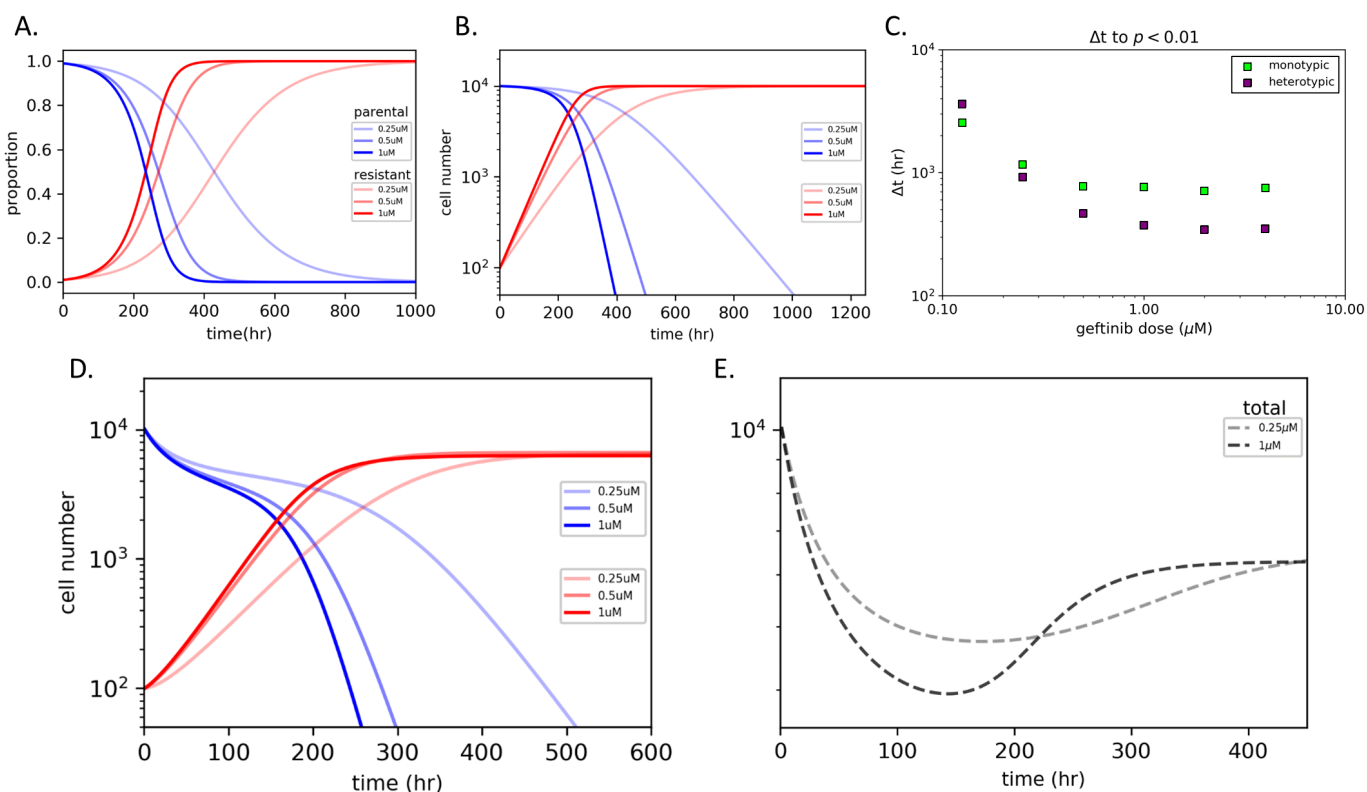


Figure 4. Evaluation of growth models with empirically derived parameters highlights rapid acceleration of competitive release via non-cell autonomous interactions and demonstrates persistence of qualitative features across the spectrum of models tested.

The same initial parameters were used for each model ($p = 0.99$). A. Replicator dynamics showing proportional shifts of both competing cell populations over time in three gefitinib doses. B. Lotka-Volterra (LV) model of outgrowth in constrained environments with equal carrying capacities ($K_p = K_r$). C. Time to extinction (defined as the proportion of the population, p , dropping below 0.01) across a range of gefitinib doses was determined and compared between cell autonomous (monotypic) and non-autonomous (heterotypic) growth. D. LV model with unequal carrying capacities ($K_i = K_{max} \alpha_i$ where $\alpha_i = r_{mono}/r_{max}$). E. Estimates for changes in total tumor burden for relative LV model in 0.25 μ M and 1 μ M of gefitinib. Treatment with the lower dose of 0.25 μ M had a smaller initial response to therapy, but longer overall response due to delayed sensitive extinction and maintenance of heterogeneity over a longer period of time.

117 While LV models can be quite sensitive to user-chosen carrying capacities, when the carrying capacities of both subclones

118 are equal ($K_p = K_r = K_{max}$), heterogeneity was maintained at identical time scales when compared to the replicator equations.
119 To evaluate the impact of frequency-dependent growth, the results were contrasted between models run with monotypic
120 culture growth parameters and those measured in heterotypic cultures (Fig 4C). Interestingly, the model predicts that as drug
121 concentration increases, the monotypic growth rates increasingly overestimates the time to extinction of the ancestor population
122 when compared to the more accurate heterotypic growth data. This is because the heterotypic data captures the accelerated rate
123 of competitive exclusion that occurs as a result of ecological effects. That is, the difference between the resistant and sensitive
124 growth rates is larger at every population fraction than the measured monotypic growth rates.

125 Because the assumption of equal carrying capacity may not be true of *in vivo* contexts, we varied the relative carrying
126 capacity of the two population to be a ratio of the monotypic growth rates, scaled by their maximum rate in the absence of
127 treatment (Fig 4D). Promisingly, these results are qualitatively identical to the results gathered from using equal carrying
128 capacity LV models, and those predicted from replicator dynamics. However, clinical tumor burden is likely most correlated
129 with the total tumor size, and not the size of a particular sub-population. With this in mind we show sample time traces of total
130 tumor population over time in response to two drug concentrations (Fig 4E). Interestingly, we observe that while a lower drug
131 concentration may lead to a smaller initial tumor decline than a larger drug concentration, the lower concentration leads to a
132 prolonged heterogeneous, and therefore more sensitive, tumor state. This is the result of a lower dose of gefitinib prolonging
133 the competition between ancestor and resistant populations, not allowing for a competition-free expansion by the resistant
134 sub-population.

135 Resistant lineage likely driven by KRAS mutation and EGFR down-regulation

136 To characterize molecular mechanisms that mediate gefitinib resistance, we then performed whole exome and RNA sequencing,
137 comparing resistant cells with parental and sensitive ones. Clonality inferences from genomic data indicated polyclonal
138 composition of ancestral cells, reflected in wide distribution of VAFs (Fig 5A, top). In contrast, distribution of VAF in resistant
139 cells displayed two clearly distinct peaks, centered around 0.5 and 0.3, suggesting a clonal origin of resistance with subsequent
140 emergence of a major sub-clone (Fig 5A, bottom). However, we are also aware of limitations of the presented results for
141 clonality estimation mainly due to copy number adjustments being relative to ancestral line and being regional estimates
142 rather than allelic copy number estimates required for a proper CCF transformation hence we limited ourselves to a qualitative
143 description based on the variation of transformed CCF values. Notably, resistant cells harbor clonal KRASG12D mutation
144 which was previously shown to cause strong gefitinib resistance⁴⁸. Given that KRAS G12D is a strong oncogenic driver^{48,49},
145 this mutation likely converted PC9 cells from EGFR dependence to KRAS dependence. Consistent with this notion, resistant
146 cells down regulated EGFR expression, while up-regulating expression of KRAS (Fig 5B, left, Fig S6). In addition, we found
147 that resistant cells displayed several copy number gains (CCND1, GADD45A, and ARAF) and losses (RB1, FHIT, and AKT1)
148 as well as expression level changes in multiple genes (CCND1, ERBB2, and cMET), that have been previously linked to lung
149 cancer progression and therapy resistance^{50–52}. These additional changes suggest compound resistant phenotypes integrating
150 impact of multiple molecular changes.

151 Discussion

152 Our work provides an extensive quantitative study of the frequency-dependent interactions between an experimentally derived
153 gefitinib-resistant PC9 cell-line and its sensitive ancestor. We have shown that a fitness cost resulting from resistance may be
154 insufficient to result in competitive exclusion of the resistant population in the absence of drug. Instead, frequency-dependent
155 ecological interactions with the sensitive population may ameliorate the fitness cost, leading to a potential safe harbor for
156 small resistant populations. As a result, future studies focused on competitive exclusion would benefit from an examination of
157 frequency-dependent ecological interactions.

158 In addition, our work also examined how the ecological interactions may shift under increasing gefitinib doses. Our results
159 show a shift from competitive exclusion of the resistant population to a competitive exclusion of the sensitive population as
160 gefitinib dose is increased. Then, with simulations we demonstrated that the inclusion of ecological effects can significantly
161 alter calculations of sensitive extinction rate and temporal tumor burdens. Past work has shown how drug and tumor
162 microenvironments can fluctuate in space^{53,54}, suggesting that these ecological interactions are likely to fluctuate over space as
163 well. Our current work absorbs the spatial effects into the effective game measurement³⁵, but future experimental and modeling
164 work will attempt to untangle these potential spatial contributions. Finally, using whole exome and RNA sequencing, we found
165 that the resistant phenotype was likely driven by KRAS G12D, in addition to down-regulation of EGFR and up-regulation of
166 KRAS.

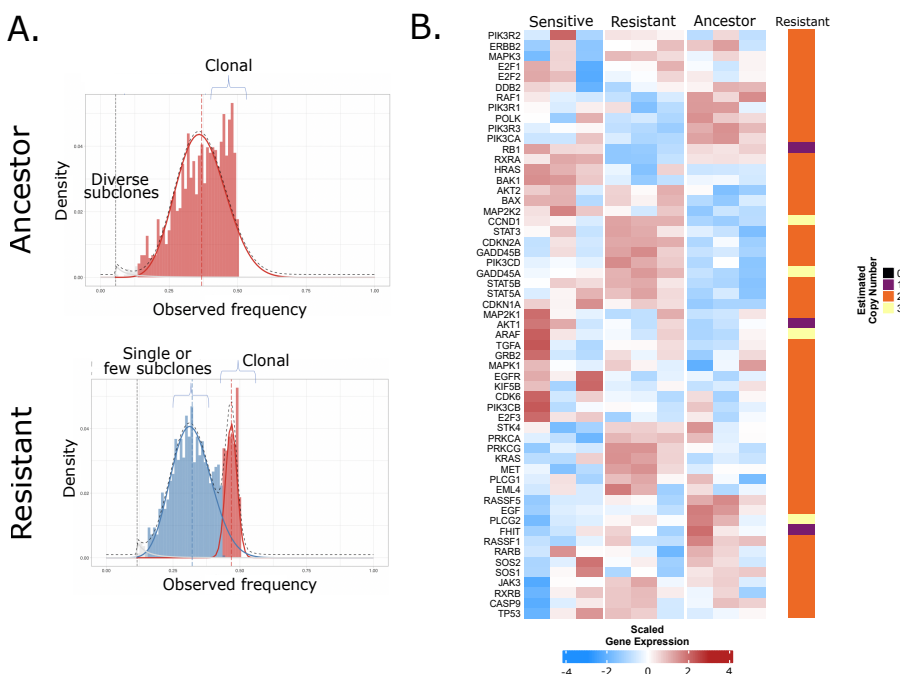


Figure 5. Sequencing shows down-regulation of EGFR and up-regulation of MET/KRAS pathways in gefitinib-resistant population. (A) Distribution of copy number and tumor purity adjusted VAFs suggesting heterogeneity of parental sample with a single wide peak and increased homogeneity for Gefitinib treated sample with 2 major narrow peaks where a major peak near 0.5 is present showing clonal mutations shared by majority of the cells in the population. (B) Three technical replicates sampled roughly a week apart were sequenced from each of the sensitive, resistant and parental/ancestral populations for RNA-Seq and single samples for WXS.

167 In interpreting our work several limitations are to be kept in mind. Measuring frequency-dependent ecological interactions
168 is extremely challenging. As such, our intention was not to produce a highly accurate, clinical model of ecological interactions
169 that can inform current cancer treatments. Instead, we focus on measuring the ecological interaction between two competing
170 populations, and how that may influence *in vitro* laboratory experiments. These experiments are a measurement of the
171 interaction between one evolved gefitinib-resistant population, in co-culture with a gefitinib-sensitive population. As such, if
172 the evolutionary process were repeated, one may measure distinctly different ecological interactions due to the stochastic nature
173 of evolution.⁵⁵ In the future we hope to measure many replicate populations to several drugs to explore the repeatability of
174 these interactions. In addition, our experimental analysis is restricted to exponential growth phase, ignoring the effects of carry
175 capacity and confluence which may play a significant role in similar experiments performed in mice or real-world observations
176 in humans. In beginning to understand this more idealized scenario we hope to understand more general principles that can be
177 tested in more complex models of resistance and ecological interactions. With that said, it is our hope to build on this simple
178 model to account for more complex interactions.

179 While our work compliments recent studies on competitive exclusion and evolutionary game theory, it also raises interesting
180 new questions for future work. For example, clinical tumors are highly heterogeneous. Extending this work to include three⁵⁶
181 or more types will allow us to better model more clinically relevant resistance evolution. Finally, our results suggest that
182 ecological effects are an important consideration in competition experiments, and continuing to show this empirically remains a
183 priority going forward.

184 Methods

185

186 **RNA-sequencing prep:** Quality control of total RNA samples is executed using Qubit Fluorometer (Invitrogen) for RNA
187 quantification and Fragment Analyzer 5200 (Agilent) to assess RNA quality using a cut-off of RIN > 7.0 to select specimens
188 for further analysis. The NEBNext rRNA Depletion Kit v2 (Human/Mouse/Rat) (New England Biolabs) is completed first. The
189 rRNA-depleted RNA is used as input for the NEBNext Ultra II Directional RNA Library Prep kit for Illumina (New England
190 BioLabs) in which libraries are tagged with unique adapter-indexes. Final libraries are validated on the Fragment Analyzer,
191 quantified via qPCR, and pooled at equimolar ratios. Pooled libraries are diluted, denatured and loaded onto the Illumina
192 NextSeq 550 system, following the NextSeq User Guide for a paired-end 75 cycle run.

193

194 **Whole exome sequencing prep:** Quality control of genomic DNA samples is executed using Qubit dsDNA BR Assay Kit
195 (Invitrogen, USA) and running on a 2% Agarose Gel. Only DNA of high quality is selected. DNA is diluted to 5 ng/μl and a
196 total of 50 ng DNA is processed using the Nextera Rapid Capture Exome kit (Illumina, San Diego, CA). This protocol starts by
197 enzymatically shearing the DNA and tagging each sample with a unique index-adapter necessary for sequencing. Final libraries
198 are purified, quantified using the Qubit dsDNA BR Assay Kit, and pooled in sets of 12, using 500 ng of each tagged library.
199 Each pool of libraries undergoes hybridization and targeted capture of the exome. Final library captures are validated using
200 the Fragment Analyzer (Agilent) and quantified via qPCR (New England BioLabs). Library pools are diluted, denatured, and
201 loaded onto the Illumina NextSeq system, following the NextSeq User Guide, for a paired-end 76 cycle run.

202 **Cell lines:** All cells were cultured in Roswell Park Memorial Institute (RPMI) media supplemented with 10% fetal bovine
203 serum (FBS) and 1% penicillin/streptomycin. Sensitive and resistant cell lines were established from the same ancestral

204 population of PC9 cells (Sigma-Aldrich 90071810). Resistant population was cultured in 1uM of gefitinib (Cayman 13166) for
205 greater than 6 months, until a population of stably growing cells was observed. Resulting subpopulations exhibited noticeable
206 visual morphological differences in culture. The sensitive population was cultured in parallel in matched volumes of dimethyl
207 sulfoxide (DMSO) (Sigma-Aldrich 276855) for the same duration as a vehicle control.

208 Resulting resistant and sensitive subclones underwent lentiviral transduction with plasmid vectors encoding EGFP- and
209 mCherry- fluorescent proteins with attached nuclear localization sequence (plasmids were a gift from Andriy Marusyk's lab at
210 Moffitt Cancer Center). Derivative cell lines with heritable fluorescent protein expression were selected for in puromycin (MP
211 Biomedical 100552).

212 **Sequencing methods:** Paired-end whole exome sequencing reads (WES) of Parental, Sensitive and Resistant populations
213 were processed to filter, align and call variants using fastp, bwa-mem, Strelka2 and GATK respectively. Read filtering with fastp
214 included low-complexity filters followed by alignment with bwa-mem with minimum seed length set to 17. Variant calls with
215 Strelka2 was run using default parameters and GATK pipeline was run according to the best-practices workflows⁵⁷⁻⁵⁹. Variant
216 calls passing default filters from 2 methods were intersected and filtered for low allelic depth. Variants are further annotated
217 for functional consequences using Ensembl VEP tool and associated publications are mined using LitVar^{60,61}. Whole exome
218 sequencing reads are further processed to identify copy-numbers using CNVkit pipeline with default parameters and using
219 DMSO treated and sensitive samples to build a reference copy-number profile. Copy-numbers are called by default threshold
220 values of \log_2 read depth ratios⁶². RNA-Seq quantification and analysis was done using Salmon, tximport, edgeR tools⁶³⁻⁶⁵.
221 Additionally, we generated distribution of cancer cell fractions (CCF) (scaled to 0-0.5), in other words, variant allele frequencies
222 (VAF) are adjusted for copy number estimates and assuming tumor purity 1.0 following the same 'multiplicity' strategy⁶⁶.
223 Scaling to 0-0.5 is done in order to represent the CCF as a pseudo VAF for input to MOBSTER package, hence 0.5 is a proxy
224 for clonal mutations in a diploid region⁶⁷. Furthermore, coupling the CCF values with MOBSTER in order to in order to assess
225 heterogeneity of mutations focusing on regions with high coverage (depth > 150) across the exome [66]. No other filtering of
226 mutation calls is done.

227 **Experimental design:** Cells were harvested at 70-80% confluence, stained with trypan blue (Corning 25-900-CI), and
228 manually counted with a hemocytometer (Bright-Line Z359629). Mono- and co-cultures of each subclone were seeded across a
229 range of initial relative proportions, totaling 3000 cells/well, in 96-well formats and allowed to attach for 18-24 hours.

230 Wells were treated with the following drugs: gefitinib, paclitaxel (Cayman 10461), etoposide (Cayman 12092), pemetrexed
231 (Cayman 26677), and lapatinib (Cayman 11493) as single agents. Plates were loaded into a BioSpa 8 Automated Incubator
232 (BioTek Instruments). Time-lapse microscopy images were obtained for bright field, GFP, and mCherry via Cytation 5 Imaging
233 Reader (BioTek) every 4 hours over the course of 5 days.

234 **Image Processing:** Images were processed with Gen5 (BioTek) and the open-source software ImageJ.⁶⁸ Image sets were
235 duplicated, background subtracted, contrasted limited adaptive histogram equalization (CLAHE), and thresholded. Despeckle
236 filter was applied to the now binary images, watershed segmentation was performed, and raw cell numbers were extracted from
237 the resulting image sets.

238 **Evolutionary Game Assay:** To quantify the dynamics in our *in vitro* environments, we used the experimental game assay
239 developed by Kaznatcheev et al.³⁰. Initial proportions were calculated for each well individually from the first image. Time
240 series of raw cell numbers were normalized against initial number in each well. Linear regression was performed using the
241 Theil-sen estimator on the semi-log cell change against time. The slope of the resulting linear function (with its corresponding
242 95% confidence interval) was translated as the growth rate across the time series, which were normalized against the average of
243 six sensitive monoculture wells that were run on each plate.

244 To find the dependence of fitness on the frequency of subclonal interaction, least squares regressions were performed on the
245 growth rate against the initial proportion of sensitive in each well. This regression was weighted against the inverse of the errors
246 ($\frac{1}{\sigma^2}$) associated with each growth rate. The resulting linear equations describe fitness as a function of the initial proportion of
247 the opposing subclone:

$$\hat{w}_P = A + kr \quad (1)$$

$$\hat{w}_R = D + kp \quad (2)$$

248 The intercepts of these functions translate to monoculture fitness, which are the symmetric payoffs within a game matrix. The
249 asymmetric payoffs can be translated as the fitness values when r and p are equal to 1:

$$B = A + k$$

$$C = D + k$$

250 These linear equations can be rearranged to describe the fitness (\hat{w}) of a sub clone as a function of the initial proportion (p) of
251 interacting cells within the population.

$$\hat{w}_P = Ap + B(1 - p)$$

$$\hat{w}_R = Cp + D(1 - p)$$

252 Payoff matrices corresponding to each of the different conditions can be derived by setting p equal to one and zero for both
253 equations. For example, the symmetric payoff for sensitive occurs when $p = 1$, which translates to $\hat{w}_P = A$.

$$\begin{matrix} & \text{P} & \text{R} \\ \text{P} & \begin{pmatrix} A & B \\ C & D \end{pmatrix} \\ \text{R} & & \end{matrix}$$

254 The errors associated with the on-diagonal payoffs are equivalent to the uncertainty of the intercept values, σ_A and σ_D for
255 sensitive and resistant respectively. The errors associated with the off-diagonal payoffs were derived by propagating the
256 uncertainty of both the intercept and slope through both the intercept and slope of (eq. 3):

$$\sigma_B = \sigma_A + \sigma_k \quad (3)$$

$$\sigma_C = \sigma_D + \sigma_k \quad (4)$$

257 **Growth models:** To synthesize hypothetical tumor growth using our measured frequency-dependent growth rates, we used
258 two distinct models, one that allowed for infinite growth and one that limited total volume to a strict maximum. This was
259 done to identify salient qualitative features that persisted across this spectrum of models, rather than make specific quantitative
260 predictions.

261 For infinite growth, replicator dynamics were chosen:

$$\dot{p} = p(\hat{w}_P - \langle w \rangle) \quad (5)$$

$$\dot{r} = (1 - p)(\hat{w}_R - \langle w \rangle) \quad (6)$$

262 where $\langle w \rangle$ denotes average population fitness (i.e., $\langle w \rangle = pw_P + (1 - p)w_R$).

263 For growth that is strictly limited to a maximum, we used a Lotka-Volterra model⁶⁹ with frequency-dependent growth:

$$\frac{dN_p}{dt} = r_p \left[1 - \frac{N_p}{K_p} - \frac{N_r r_r}{K_p r_p} \right] N_p \quad (7)$$

$$\frac{dN_r}{dt} = r_r \left[1 - \frac{N_r}{K_r} - \frac{N_p r_p}{K_r r_r} \right] N_r \quad (8)$$

264 where r_p and r_r are non-cell autonomous growth rates determined by values of the game matrix such that:

$$r_p = A \left(\frac{N_p}{N_p + N_r} \right) + B \left(\frac{N_r}{N_p + N_r} \right) \quad (9)$$

$$r_r = C \left(\frac{N_p}{N_p + N_r} \right) + D \left(\frac{N_r}{N_p + N_r} \right) \quad (10)$$

265 While this model is insensitive specific carrying capacity values, it is highly sensitive to the relative value of the carrying
266 capacity. Given that both subclones occupy similar space in an *in vitro* environment, we first evaluated the condition where
267 the carrying capacities were equal to one another ($K_p = K_r$). This assumption likely does not translate to *in vivo* conditions.
268 Instead, the carrying capacities of each type would likely vary across different environments. To capture this phenomenon, the
269 carrying capacity was also scaled for each condition:

$$K_i = K_{max} \alpha_i \quad (11)$$

270 where K_{max} is the maximum carrying capacity across all conditions and α_i is a weighting term that scales this maximum using
271 a ratio of monoculture growth rate in the current condition against the maximum growth rate $\alpha_i = \frac{r_{mono}}{r_{max}}$.

272 **Acknowledgements:** This research was supported by the Genomics Core Facility of the CWRU School of Medicine's
273 Genetics and Genome Sciences Department and made use of the High Performance Computing Resource in the Core Facility
274 for Advanced Research Computing at Case Western Reserve University.

275 **Funding:** This study was supported by the National Institutes of Health (5R37CA244613-02) and the American Cancer Society
276 Research Scholar Grant (RSG-20-096-01).

277 **Author Contributions:** Conceptualization: N.F., J.M., A.M., A.K., J.S. Methodology: N.F., J.M., A.D., A.M., A.K., J.S.,
278 Investigation: N.F., J.M., M.D., A.D., P.E., M.H., E.M., A.M., A.K., J.S., Visualization: N.F., J.M., A.D., A.M., A.K., J.S., Data
279 Scoring and Analysis: N.F., J.M., A.D., A.M., Writing, Original Draft: N.F., J.M., J.S. Writing, Review and Editing: N.F., J.M.,
280 M.D., A.D., P.E., M.H., E.M., A.M., A.K., J.S., Supervision: A.M., A.K., J.S.

281 **Competing Interests:** The authors declare no competing interests.

282 **Data and Materials Availability:** All data needed to evaluate the conclusions in the paper are present in the paper and/or the
283 Supplementary Materials. Relevant sequencing has been uploaded to the SRA, accession number: PRJNA801780.

References

1. Cahill, D. P., Kinzler, K. W., Vogelstein, B. & Lengauer, C. Genetic instability and darwinian selection in tumours. *Trends cell biology* **9**, M57–M60 (1999).
2. Loeb, L. A. Mutator phenotype may be required for multistage carcinogenesis. *Cancer research* **51**, 3075–3079 (1991).
3. Marusyk, A., Almendro, V. & Polyak, K. Intra-tumour heterogeneity: a looking glass for cancer? *Nat. Rev. Cancer* **12**, 323–334 (2012).
4. Almendro, V., Marusyk, A. & Polyak, K. Cellular heterogeneity and molecular evolution in cancer. *Annu. Rev. Pathol. Mech. Dis.* **8**, 277–302 (2013).
5. Loeb, L. A. Human cancers express a mutator phenotype: hypothesis, origin, and consequences. *Cancer research* **76**, 2057–2059 (2016).
6. McGranahan, N. & Swanton, C. Biological and therapeutic impact of intratumor heterogeneity in cancer evolution. *Cancer cell* **27**, 15–26 (2015).
7. Gerlinger, M. *et al.* Intratumor heterogeneity and branched evolution revealed by multiregion sequencing. *N Engl J Med* **366**, 883–892 (2012).
8. Burrell, R. A., McGranahan, N., Bartek, J. & Swanton, C. The causes and consequences of genetic heterogeneity in cancer evolution. *Nature* **501**, 338–345 (2013).
9. Marusyk, A. *et al.* Non-cell-autonomous driving of tumour growth supports sub-clonal heterogeneity. *Nature* **514**, 54–58 (2014).
10. Axelrod, R., Axelrod, D. E. & Pienta, K. J. Evolution of cooperation among tumor cells. *Proc. Natl. Acad. Sci.* **103**, 13474–13479 (2006).
11. Dujon, A. M. *et al.* Identifying key questions in the ecology and evolution of cancer. *Evol. applications* **14**, 877–892 (2021).
12. Wölfel, B. *et al.* The contribution of evolutionary game theory to understanding and treating cancer. *Dyn. Games Appl.* 1–30 (2021).
13. Zheng, Y., Sun, Y., Torga, G., Pienta, K. & Austin, R. Game theory cancer models of cancer cell-stromal cell dynamics using interacting particle systems. *Biophys. Rev. Lett.* **15**, 171–193 (2020).
14. Lotka, A. J. Analytical note on certain rhythmic relations in organic systems. *Proc. Natl. Acad. Sci.* **6**, 410–415 (1920).
15. Lima, S. L. Putting predators back into behavioral predator–prey interactions. *Trends Ecol. & Evol.* **17**, 70–75 (2002).
16. Basanta, D. *et al.* Investigating prostate cancer tumour–stroma interactions: clinical and biological insights from an evolutionary game. *Br. journal cancer* **106**, 174–181 (2012).
17. Pacheco, J. M., Santos, F. C. & Dingli, D. The ecology of cancer from an evolutionary game theory perspective. *Interface focus* **4**, 20140019 (2014).
18. Archetti, M. & Pienta, K. J. Cooperation among cancer cells: applying game theory to cancer. *Nat. Rev. Cancer* **19**, 110–117 (2019).
19. Bohl, K. *et al.* Evolutionary game theory: molecules as players. *Mol. BioSystems* **10**, 3066–3074 (2014).
20. Kaznatcheev, A. Evolution is exponentially more powerful with frequency-dependent selection. *bioRxiv* 2020–05 (2021).
21. Basanta, D., Gatenby, R. A. & Anderson, A. R. Exploiting evolution to treat drug resistance: combination therapy and the double bind. *Mol. pharmaceutics* **9**, 914–921 (2012).
22. Basanta, D. & Anderson, A. R. Exploiting ecological principles to better understand cancer progression and treatment. *Interface focus* **3**, 20130020 (2013).
23. Janiszewska, M. *et al.* Subclonal cooperation drives metastasis by modulating local and systemic immune microenvironments. *Nat. cell biology* **21**, 879–888 (2019).
24. Martin, R. B. Optimal control drug scheduling of cancer chemotherapy. *Automatica* **28**, 1113–1123 (1992).
25. Yurtsev, E. A., Chao, H. X., Datta, M. S., Artemova, T. & Gore, J. Bacterial cheating drives the population dynamics of cooperative antibiotic resistance plasmids. *Mol. systems biology* **9**, 683 (2013).
26. Enriquez-Navas, P. M. *et al.* Exploiting evolutionary principles to prolong tumor control in preclinical models of breast cancer. *Sci. translational medicine* **8**, 327ra24–327ra24 (2016).

27. Zhang, J., Cunningham, J. J., Brown, J. S. & Gatenby, R. A. Integrating evolutionary dynamics into treatment of metastatic castrate-resistant prostate cancer. *Nat. communications* **8**, 1–9 (2017).
28. Warman, P. I., Kaznatcheev, A., Araujo, A., Lynch, C. C. & Basanta, D. Fractionated follow-up chemotherapy delays the onset of resistance in bone metastatic prostate cancer. *Games* **9**, 19 (2018).
29. Maltas, J. & Wood, K. B. Pervasive and diverse collateral sensitivity profiles inform optimal strategies to limit antibiotic resistance. *PLOS Biol.* **17**, 1–34, DOI: [10.1371/journal.pbio.3000515](https://doi.org/10.1371/journal.pbio.3000515) (2019).
30. Kaznatcheev, A., Peacock, J., Basanta, D., Marusyk, A. & Scott, J. G. Fibroblasts and alectinib switch the evolutionary games played by non-small cell lung cancer. *Nat. ecology & evolution* **3**, 450–456 (2019).
31. Viossat, Y. & Noble, R. A theoretical analysis of tumour containment. *Nat. Ecol. & Evol.* **5**, 826–835 (2021).
32. Gluzman, M., Scott, J. G. & Vladimirska, A. Optimizing adaptive cancer therapy: dynamic programming and evolutionary game theory. *Proc. Royal Soc. B* **287**, 20192454 (2020).
33. Maltas, J. & Wood, K. B. Dynamic collateral sensitivity profiles highlight challenges and opportunities for optimizing antibiotic sequences. *bioRxiv* (2021).
34. Kaznatcheev, A. Two conceptions of evolutionary games: reductive vs effective. *bioRxiv* 231993 (2017).
35. Kaznatcheev, A. Effective games and the confusion over spatial structure. *Proc. Natl. Acad. Sci.* **115**, E1709–E1709 (2018).
36. West, J., Ma, Y. & Newton, P. K. Capitalizing on competition: An evolutionary model of competitive release in metastatic castration resistant prostate cancer treatment. *J. Theor. Biol.* **455**, 249–260 (2018).
37. Connell, J. H. The influence of interspecific competition and other factors on the distribution of the barnacle chthamalus stellatus. *Ecology* **42**, 710–723 (1961).
38. Hansen, E., Karslake, J., Woods, R. J., Read, A. F. & Wood, K. B. Antibiotics can be used to contain drug-resistant bacteria by maintaining sufficiently large sensitive populations. *PLOS Biol.* **18**, 1–20, DOI: [10.1371/journal.pbio.3000713](https://doi.org/10.1371/journal.pbio.3000713) (2020).
39. Wargo, A. R., Huijben, S., De Roode, J. C., Shepherd, J. & Read, A. F. Competitive release and facilitation of drug-resistant parasites after therapeutic chemotherapy in a rodent malaria model. *Proc. Natl. Acad. Sci.* **104**, 19914–19919 (2007).
40. Huijben, S. *et al.* Aggressive chemotherapy and the selection of drug resistant pathogens. *PLoS Pathog* **9**, e1003578 (2013).
41. Pollitt, L. C. *et al.* Rapid response to selection, competitive release and increased transmission potential of artesunate-selected plasmodium chabaudi malaria parasites. *PLoS Pathog* **10**, e1004019 (2014).
42. Bacevic, K. *et al.* Spatial competition constrains resistance to targeted cancer therapy. *Nat. communications* **8**, 1–15 (2017).
43. Szakacs, G. *et al.* Targeting the achilles heel of multidrug-resistant cancer by exploiting the fitness cost of resistance. *Chem. reviews* **114**, 5753–5774 (2014).
44. Chmielecki, J. *et al.* Optimization of dosing for egfr-mutant non–small cell lung cancer with evolutionary cancer modeling. *Sci. translational medicine* **3**, 90ra59–90ra59 (2011).
45. Pena, J., Lehmann, L. & Nöldeke, G. Gains from switching and evolutionary stability in multi-player matrix games. *J. Theor. Biol.* **346**, 23–33 (2014).
46. Karslake, J., Maltas, J., Brumm, P. & Wood, K. B. Population density modulates drug inhibition and gives rise to potential bistability of treatment outcomes for bacterial infections. *PLoS computational biology* **12**, e1005098 (2016).
47. Gerlee, P. & Altrock, P. M. Extinction rates in tumour public goods games. *J. The Royal Soc. Interface* **14**, 20170342 (2017).
48. Ali, M. *et al.* Codon bias imposes a targetable limitation on kras-driven therapeutic resistance. *Nat. communications* **8**, 1–11 (2017).
49. Guerra, C. *et al.* Tumor induction by an endogenous k-ras oncogene is highly dependent on cellular context. *Cancer cell* **4**, 111–120 (2003).
50. Friese-Hamim, M., Bladt, F., Locatelli, G., Stammberger, U. & Blaukat, A. The selective c-met inhibitor tepotinib can overcome epidermal growth factor receptor inhibitor resistance mediated by aberrant c-met activation in nsclc models. *Am. journal cancer research* **7**, 962 (2017).

51. Erjala, K. *et al.* Signaling via erbB2 and erbB3 associates with resistance and epidermal growth factor receptor (EGFR) amplification with sensitivity to EGFR inhibitor gefitinib in head and neck squamous cell carcinoma cells. *Clin. Cancer Res.* **12**, 4103–4111 (2006).
52. Kalish, L. H. *et al.* Deregulated cyclin D1 expression is associated with decreased efficacy of the selective epidermal growth factor receptor tyrosine kinase inhibitor gefitinib in head and neck squamous cell carcinoma cell lines. *Clin. cancer research* **10**, 7764–7774 (2004).
53. Scott, J. G., Hjelmeland, A. B., Chinnaiyan, P., Anderson, A. R. A. & Basanta, D. Microenvironmental variables must influence intrinsic phenotypic parameters of cancer stem cells to affect tumourigenicity. *PLOS Comput. Biol.* **10**, 1–7, DOI: [10.1371/journal.pcbi.1003433](https://doi.org/10.1371/journal.pcbi.1003433) (2014).
54. Kim, M., Gillies, R. J. & Rejniak, K. A. Current advances in mathematical modeling of anti-cancer drug penetration into tumor tissues. *Front. oncology* **3**, 278 (2013).
55. Blount, Z. D., Borland, C. Z. & Lenski, R. E. Historical contingency and the evolution of a key innovation in an experimental population of *Escherichia coli*. *Proc. Natl. Acad. Sci.* **105**, 7899–7906 (2008).
56. Bhattacharya, R. *et al.* Understanding the evolutionary games in NSCLC microenvironment. *bioRxiv* (2020).
57. McKenna, A. *et al.* The genome analysis toolkit: a mapreduce framework for analyzing next-generation DNA sequencing data. *Genome research* **20**, 1297–1303 (2010).
58. Kim, S. *et al.* Strelka2: fast and accurate calling of germline and somatic variants. *Nat. methods* **15**, 591–594 (2018).
59. Li, H. Aligning sequence reads, clone sequences and assembly contigs with bwa-mem. *arXiv preprint arXiv:1303.3997* (2013).
60. McLaren, W. *et al.* The Ensembl variant effect predictor. *Genome biology* **17**, 1–14 (2016).
61. Allot, A. *et al.* Litvar: a semantic search engine for linking genomic variant data in PubMed and PMC. *Nucleic acids research* **46**, W530–W536 (2018).
62. Talevich, E., Shain, A. H., Botton, T. & Bastian, B. C. Cnvkit: genome-wide copy number detection and visualization from targeted DNA sequencing. *PLoS computational biology* **12**, e1004873 (2016).
63. Robinson, M. D., McCarthy, D. J. & Smyth, G. K. edger: a Bioconductor package for differential expression analysis of digital gene expression data. *Bioinformatics* **26**, 139–140 (2010).
64. Love, M. I., Soneson, C. & Robinson, M. D. Importing transcript abundance datasets with tximport. *Dim Tx. Inf. Rep. Sample1* **1**, 5 (2017).
65. Patro, R., Duggal, G. & Kingsford, C. Salmon: accurate, versatile and ultrafast quantification from RNA-seq data using lightweight-alignment. *BioRxiv* 021592 (2015).
66. Dentro, S. C., Wedge, D. C. & Van Loo, P. Principles of reconstructing the subclonal architecture of cancers. *Cold Spring Harb. perspectives medicine* **7**, a026625 (2017).
67. Caravagna, G., Sanguinetti, G., Graham, T. A. & Sottoriva, A. The mobster R package for tumour subclonal deconvolution from bulk DNA whole-genome sequencing data. *BMC bioinformatics* **21**, 1–11 (2020).
68. Schindelin, J. *et al.* Fiji: an open-source platform for biological-image analysis. *Nat. methods* **9**, 676–682 (2012).
69. Li, X.-Y. *et al.* Which games are growing bacterial populations playing? *J. The Royal Soc. Interface* **12**, 20150121 (2015).

Supplemental Information

Evolutionary Game Assay

To quantify the dynamics in our *in vitro* environments, we used the experimental game assay developed by Kaznatcheev et al.³⁰.

Tracking individual subclones in heterotypic cultures: To track differential growth dynamics of two populations in the same culture, each population was transduced with a vector encoding a different heritable fluorescent protein. For this experiment, the resistant and sensitive cells were made to stably express mCherry and EGFP respectively. The expression of these proteins was linked to nuclear localization signal (NLS) repeats for localization of the fluorescent signal into each cell's nuclei. This increases resolution and accuracy of cell number counts at higher confluence. Once plated together in heterotypic culture, each subclone could be tracked through time in their respective fluorescent channel using time-lapse microscopy systems (**Fig 1A**).

Translating image information into growth rates: Cell number counts were extracted from each fluorescent image at each time point throughout the time series. Exponential growth rates were determined via semi-log regression of change in cell number against change in time (hours) using the Theil-sen estimator (**Fig 1B**).

Fitness functions - growth as a function of population composition: To find the dependence of fitness on the frequency of subclonal interaction, least squares regressions were performed on the growth rate against the initial proportion of sensitive in each well (**Fig 1C**). This regression was weighted against the inverse of the errors ($\frac{1}{\sigma^2}$) associated with each growth rate. The resulting linear equations describe growth (\hat{w}_S, \hat{w}_R) as a function of the initial proportion of the opposing subclone (in our case, p represents the sensitive proportion of the population, or $\frac{N_S}{N_T}$, where N_S is the sensitive population size and N_T is the total population size):

$$\hat{w}_S = Ap + B(1 - p) \quad (\text{S1})$$

$$\hat{w}_R = Cp + D(1 - p) \quad (\text{S2})$$

Game theoretical payoff matrix: To clearly represent the fitness outcome of specific interactions, payoff matrices corresponding to each of the different conditions can be derived from the resulting fitness functions (**Fig 1D**). For example, the fitness outcome of sensitive cells interacting with one another occurs when $p = 1$, which translates to $\hat{w}_S = A$. Similarly, the fitness outcome of when sensitive interacts with resistant occurs when $p = 0$, which translates to $\hat{w}_S = B$.

$$\begin{array}{cc} & \text{S} \quad \text{R} \\ \text{S} & \left(\begin{array}{cc} A & B \\ C & D \end{array} \right) \\ \text{R} & \end{array} \quad (\text{S3})$$

For more details on the game assay, see Kaznatcheev et al.³⁰ for method and Kaznatcheev³⁴ for interpretation.

Studying the effect of density dependence on monoculture growth rates

Our findings of frequency dependent changes in growth rate in co-culture could, in theory, have been affected by pure density dependent effects. To tease apart these two effects, we performed a monoculture experiment over a range of initial seeding densities following a 2-fold dilution pattern ranging from 3,000 cells/well to 187 cells/well.

In **Supplemental Figure S1**, we show that both the sensitive and resistant strains have a slight positive density-dependence to their growth rate. However, based on our game-assay data, the resistant (red) population would have to have a large *negative* density-dependence for density effects to be responsible for our observed game phenotype. This is because as the resistant population gets smaller (approaches a $p = 1$ fraction), we observed an increase in growth rate, the opposite of the density effect we observed. Experiments in the main draft were plated at approximately 1500 cells and thus closely match in initial and final cell counts here.

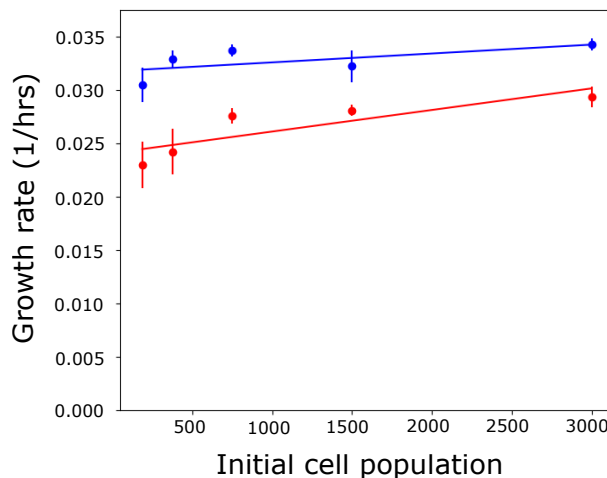


Figure S1. Monoculture density-dependence does not explain the observed co-culture dynamics. Monoculture sensitive (blue) and resistant (red) populations were plated in two fold dilutions ranging from approximately 200 to 3,000 initial populations. These monoculture measurements indicate a slightly positive effect of density on growth for both sensitive and resistant populations.

Growth curves suggest pure exponential growth fit is insufficient in co-culture.

Here we confirm the effect of ecological dynamics on the growth of the population through an alternate method. Using a large and diverse collection of initial co-culture frequencies grown in DMSO, we fit each growth curve with an exponential that assumes the growth rates are simply what was measured in mono-culture. Put another way, we assume there are no ecological interactions **Supplemental Figure S2**. We can observe by eye that the exponential fit is best in the case of no ecological interactions (that is, monoculture growth). To confirm this we plot the residuals for each plot (Observed cell count at t=80h - Predicted cell count at t=80h via no ecological interactions) **Supplemental Figure S3**. We see the residuals are minimized in the case of monoculture experiments (initial resistant fraction of 0.0 or 1.0.) and largest in co-culture. In addition, the residuals measured are all positive, suggesting the ecological interactions are spurring greater growth than predicted by monoculture alone, which matches the positive growth effect on co-culture we observe in the main draft.

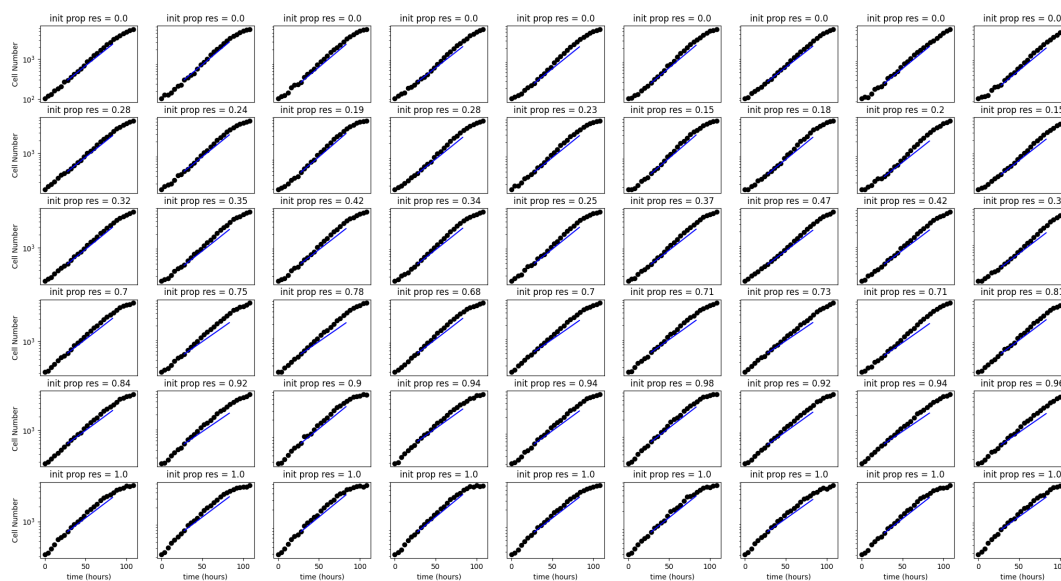


Figure S2. Monoculture growth rates are bad predictors of co-culture growth curves. Raw cell count over time (growth curves) for a collection of varied initial resistance fraction ranging from 0.0 to 1.0. Blue line on each plot represents a predicted growth curve based on monoculture growth rates (or an absence of ecological interactions).

Raw data from competition experiments

For ease of visualization, we left out the entirety of the raw data in our main text exposition. For transparency, we include a visualization of those data here. In **Supplemental Figure S4**, we show all the raw count data (In-transformed) for the above density-dependence experiment. This is highly representative of data collected throughout the manuscript. In addition, we show the best fit regressions, showing the subsection of the data used in the analysis (represented by the red lines).

In **Supplemental Figure S5**, we then show the raw data underlying the fitted trend lines from **Figure 3** of the manuscript. These raw data were excluded from the main manuscript, as to not clutter the visual with too many overlapping error bars.

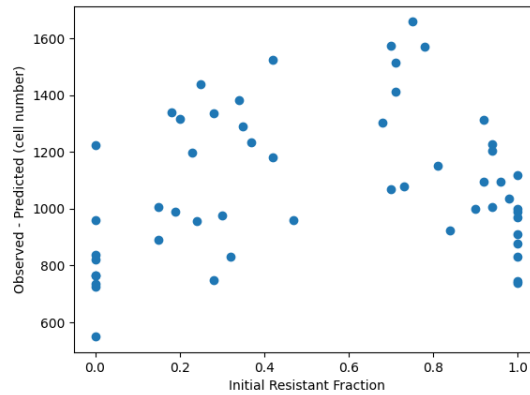


Figure S3. Residuals are maximized under co-culture and minimized under monoculture. For each initial fraction, we plot the difference between the observed cell count at 80h and the predicted cell count at 80h assuming no ecological interactions (and thus monoculture growth rate).

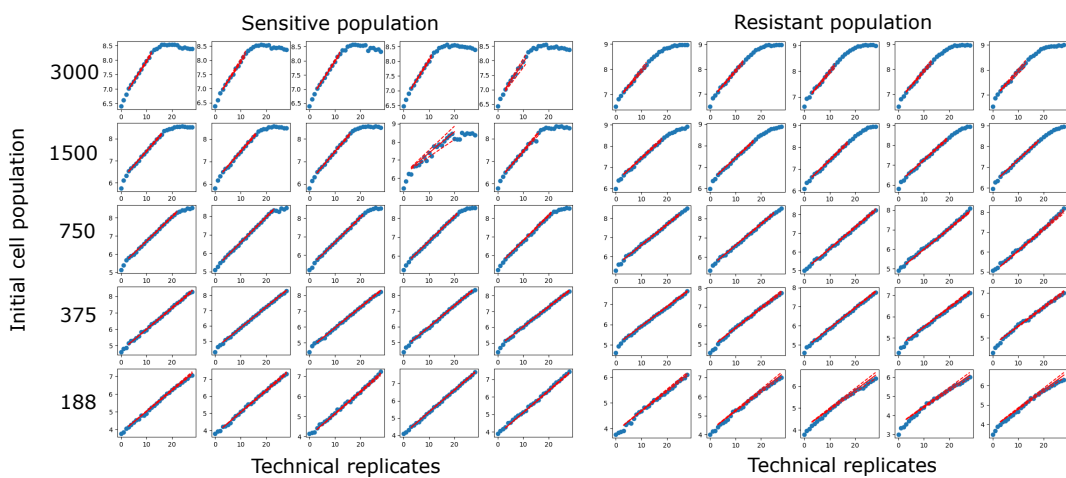


Figure S4. Typical experimental growth curves for a game assay experiment. Blue dots represent raw count data plotted on a log scale. Red best-fit regressions show the range of data used in the analysis. These data in particular are taken from the monoculture density-dependence experiment leading to Figure S1.

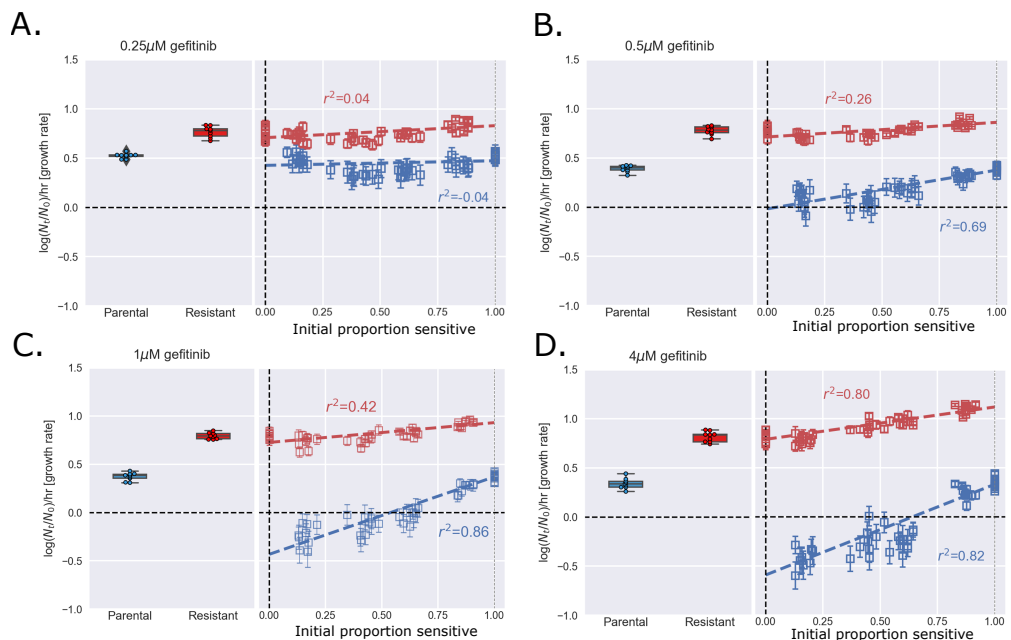


Figure S5. Raw data underlying fitted trend lines from Figure 3. **A.** Raw data underlying **Figure 3B** trend lines at $0.25\mu\text{M}$ gefitinib. **B.** Raw data underlying **Figure 3B** trend lines at $0.50\mu\text{M}$ gefitinib. **C.** Raw data underlying **Figure 3B** trend lines at $1.00\mu\text{M}$ gefitinib. **D.** Raw data underlying **Figure 3B** trend lines at $4.00\mu\text{M}$ gefitinib.

Gene expression profiling

In order to study gene expression patterns, we plot log scale fold-change values and associated *p*-values in phred scale, in **Supplemental Figure S6**, which quantifies the gene expression patterns and assesses differential regulation between sensitive and resistant populations. We show that in addition to multiple possibly relevant genes, *EGFR*, *KRAS* and *MET* show differential regulation suggestive of possible resistance associated mechanisms as given in main text.

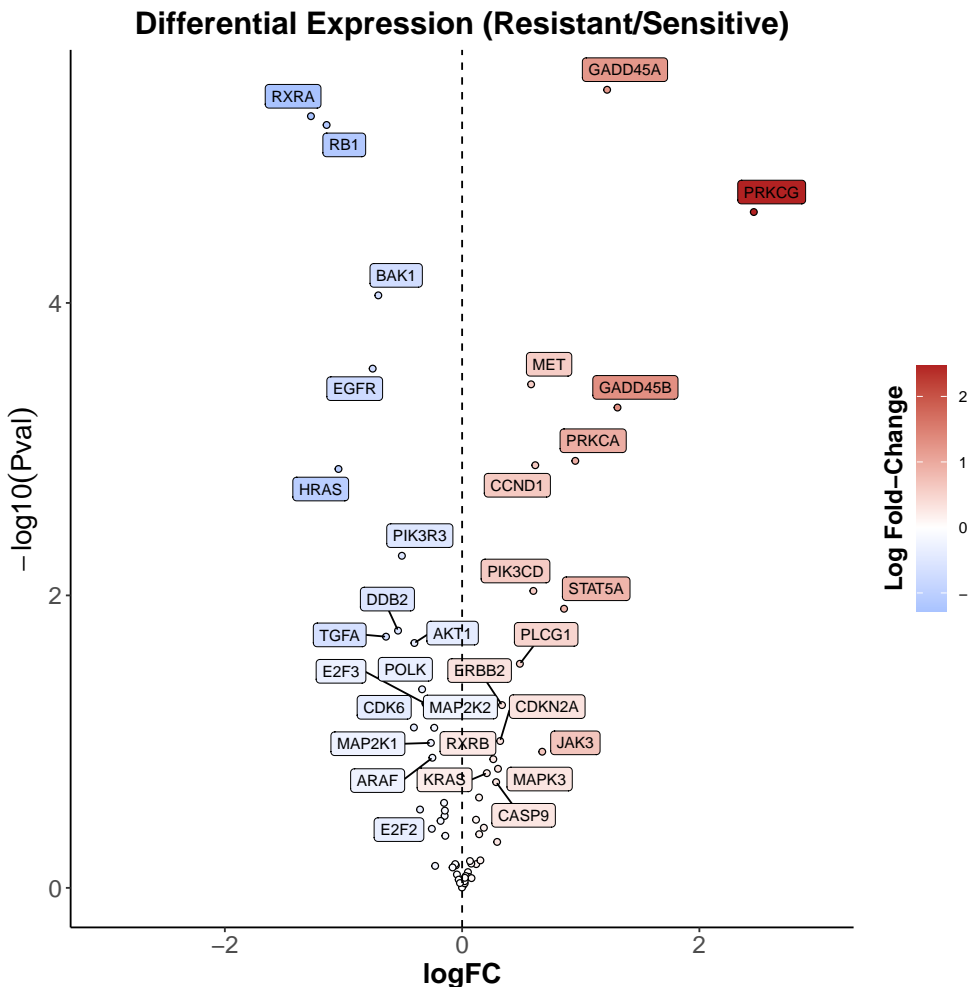


Figure S6. Differential gene expression analysis showing down/up regulation of genes in KEGG NSCLC pathway. Utilizing *edgeR* we normalized the raw counts by trimmed mean of m-values (TMM) and quantified statistical differences between sensitive and resistant populations where *EGFR* showed decreased expression in-contrast *KRAS*, *MET* genes showed increased expression.